

Prompting Medical Large Vision-Language Models to Diagnose Pathologies by Visual Question Answering

Danfeng Guo

Computer Science Department, University of California, Los Angeles, CA, USA

lyleguo@g.ucla.edu

Demetri Terzopoulos

Computer Science Department, University of California, Los Angeles, CA, USA
VoxelCloud, Inc., Los Angeles, CA, USA

dt@cs.ucla.edu

Abstract

Large Vision-Language Models (LVLMs) have achieved significant success in recent years, and they have been extended to the medical domain. Although demonstrating satisfactory performance on medical Visual Question Answering (VQA) tasks, Medical LVLMs (MLVLMs) suffer from the hallucination problem, which makes them fail to diagnose complex pathologies. Moreover, they readily fail to learn minority pathologies due to imbalanced training data. We propose two prompting strategies for MLVLMs that reduce hallucination and improve VQA performance. In the first strategy, we provide a detailed explanation of the queried pathology. In the second strategy, we fine-tune a cheap, weak learner to achieve high performance on a specific metric, and textually provide its judgment to the MLVLM. Tested on the MIMIC-CXR-JPG and Chexpert datasets, our methods significantly improve the diagnostic F1 score, with the highest increase being 0.27. We also demonstrate that our prompting strategies can be extended to general LVLm domains. Based on POPE metrics, it effectively suppresses the false negative predictions of existing LVLMs and improves Recall by approximately 0.07.

Keywords: Medical Visual Question Answering, Large Vision-Language Models, Prompt Engineering

1. Introduction

Research on Large Language Models (LLMs) has yielded astonishing results in recent years. LLMs with billions of parameters have achieved outstanding abilities in a wide range of application scenarios (OpenAI, 2022; OpenAI et al., 2023; Chiang et al., 2023). The success of LLMs has quickly extended into the Vision-Language (VL) domain. Large Vision-Language Models (LVLMs) are built upon LLMs by training adapters that project visual features into features that can be interpreted by LLMs (Li et al., 2023b; Zhang et al., 2023; Liu et al., 2023b). Visual Question Answering (VQA) is an essential skill of LVLMs, and VQA accuracy serves as a test metric for most of these models (Li et al., 2023b; Zhang et al., 2023; Zhu et al., 2023; Liu et al., 2023b). LVLMs have been pretrained on medical datasets (Li et al., 2023a; Liu et al., 2023c; Singhal et al., 2023) and they have been tested on medical VQA tasks (Lau et al., 2018; He et al., 2020). These Medical LVLMs (MLVLMs) have been able to answer questions regarding the imaging modalities, organs, and abnormalities depicted by the input medical scans.

Unfortunately, however, “hallucination” has been a major problem for LVLMs. This refers to the generation of content that is contradictory to the input images. Hallucination can be measured via VQA. One may ask the model questions regarding the existence of objects in the input image(s) and the hallucination level is assessed as the percentage of correctly answered questions. VQA can also potentially serve for medical image diagnosis. Users pose questions regarding a pathology and the MLVLM responds based on its analysis of the medical scans. However, most of the available datasets involve simple questions such as “what is the modality of this image” and “what is the organ/tissue in this image”. MLVLMs have yet to be thoroughly evaluated on VQA accuracy across a broad spectrum of pathologies. Additionally, general VQA models are usually tested by the commonly known accuracy: the percentage of correctly answered questions, which is an unsuitable measure for medical VQA. Medical image classification metrics such as the Precision, Recall, and F1 are more suitable for the evaluation of medical VQA models. Several strategies have been explored to enhance the question answering of LLMs/LVLMs, including chain-of-thought prompting (Zheng et al., 2023), self-consistency (Wang et al., 2023), and retrieval-based augmentation (Caffagni et al., 2024). All these methods involve fine-tuning the models, which is expensive. Training-free methods to improve the VQA accuracy of MLVLMs are desirable.

For MLVLMs, hallucination is exacerbated by imbalanced training data. Many pathologies are minority categories in medical datasets. Models trained on large-scale medical data may easily fail to learn the features of less common pathologies. Addressing data bias typically involves strategies such as including more data of better quality, but given the scarcity of medical data, significantly enlarging the dataset may not be feasible. Common remediations involve re-sampling the data such that the positive and negative cases are better balanced, but this poses challenges when the data involves multiple categories of pathology. Additionally, re-sampling may undermine the training needs of LVLMs, which generally require large quantities of data. These problems highlight the need of a cost-effective approach to navigate the problem of minority categories in datasets.

Our study focuses on the VQA abilities of MLVLMs. In particular, we test an existing MLVLM, LLaVA-Med (Li et al., 2023a) for chest X-ray VQA across 5 categories of pathologies. The results show that the model has low accuracy, especially on minority pathologies. To enhance its VQA accuracy, we propose two prompting strategies. The first involves enriching prompts with detailed explanations of the queried pathology. The explanations include how the queried pathology is defined and how it appears in images. Our second strategy involves introducing an auxiliary weak-learner model as another agent. We train a small image classifier and fine-tune it to identify negative images accurately. Then, the negative predictions of this classifier are appended to the prompt as a reference for the MLVLM.

We run our experiments on the MIMIC-CXR-JPG (Goldberger et al., 2000) and Chexpert (Irvin et al., 2019) datasets. The results show that our prompt strategies improve the F1 score significantly in most pathology categories (highest +0.27). We also show that our weak-learner-prompting strategy is applicable to the general domain. It reduces the false negative predictions of general domain LVLMs and improves the Recall by around 0.07 according to POPE metrics (Li et al., 2023c).

To summarize, our contributions include the following:

1. We improve the VQA accuracy of MLVLMs by prompting with detailed explanations of pathologies.
2. We introduce a low-cost weak learner model as a reference for LLaVA-Med, and this effectively reduces the false positive (FP) answers.
3. We show that our second prompting strategy can be extended to general domains to help models adapt to specialized accuracy needs.

Section 2 reviews related work, Section 3 describes our methodology, Section 4 presents our empirical study and its results, and Section 5 draws conclusions from our research.

2. Related Work

LVLMS and VQA LVLMS are built upon LLMs. A pretrained visual encoder extracts the visual features and an adapter module projects the extracted features to ones that can be understood by the LLM. Models of this type include those by Liu et al. (2023b), Zhu et al. (2023), and Zhang et al. (2023). During training, the visual encoder and the LLM are usually fixed. VQA is an essential skill of LVLMS. Given an input image, the models should be able to answer questions correctly regarding that image.

Hallucination in LVLMS VQA The hallucination problem usually refers to the LVLMS generating a response that is not consistent with the input image. For VQA, in their generated answers the models may make mistakes on object presence, location, attributes, or the mutual relationship between objects. Li et al. (2023c) find that frequently occurring objects are easily hallucinated by LVLMS, in that they tend to mention such objects even if they are absent in the image. Qian et al. (2024) and Liu et al. (2023a) show that LVLMS sometimes presume the assumptions in questions are true and easily give wrong answers when asked about some objects not in the given image.

Causes of LVLMS VQA Hallucination Hallucination can result from bias in the training data, missing fine-grained visual features, and LLM decoding strategies (Liu et al., 2024). For data bias, the imbalanced distribution of data is an important aspect. When most of the answers to a question in the training data are “Yes”, the model tends to answer “Yes” to that question. Missing fine-grained visual features usually result from the pretraining of the visual encoder. Most LVLMS use the visual encoder of CLIP trained through contrastive learning. The encoder mainly focuses on salient features and ignores fine-grained features (Jain et al., 2023). LVLMS decoding strategies mostly choose the next word as the one having maximum conditional probability given previous text and the input image. This can lead to hallucination when the model overly relies on the knowledge learned in its training texts. Other causes include model simplicity and insufficient attention (Liu et al., 2024).

Mitigation of LVLMS VQA Hallucination Strategies to mitigate hallucination in LVLMS mainly fall into two categories: prompt engineering and model improvement. Regarding the former, Liu et al. (2023a) leverage visual instructions constructed from the bounding box information in the input image to prompt LLMs. Zheng et al. (2023) use a chain of thought scheme to prompt the models to perform step-by-step visual-language reasoning like humans, which eventually leads to the correct answers. Wang et al. (2023)

generate multiple chains of thought and use the one with the majority vote as the answer. Caffagni et al. (2024) prompt the model with explanations of the terms in questions. With regard to the model improvement strategy for reducing hallucination, Sun et al. (2023b) improve the visual and text feature alignment through reinforcement learning. Leng et al. (2023) propose a contrastive decoding strategy to reduce reliance on pretrained knowledge. Favero et al. (2024) and Zhao et al. (2024) also focus on the inference stage and propose specialized decoding strategies to mitigate hallucination. Other strategies for reducing hallucination have been proposed. For example, Zhou et al. (2024) design a post-processing model to detect hallucinated objects and rephrase the generated answers, and Sun et al. (2023a) adapt a reinforcement learning strategy that uses human evaluation of the hallucination level to improve the model.

Assessment of LVL M Hallucination There are two approaches to assessing hallucination in LVL Ms. The first is VQA. The ground truth information of the input images is leveraged to construct questions regarding the existence of objects in the images (e.g., “Is there a black cat in the image?”), as well as questions about objects which do not exist in the images. The models are evaluated in terms of the percentage of correctly answered questions. Metrics of this type include POPE (Li et al., 2023c), CIEM (Hu et al., 2023), and NOPE (Lovenia et al., 2023). The second approach is to use pre-designed prompts from which the models produce various generations that are then evaluated. Examples include CHAIR (Rohrbach et al., 2018), which counts the hallucinated objects in generated image captions, and MMHAL-BENCH (Sun et al., 2023b), which uses GPT-4 (OpenAI et al., 2023) to compare the generations with human answers and determine the propensity toward hallucination.

VQA in MLVLMs For MLVLMs, given a medical scan, models such as LLaVA-Med (Li et al., 2023a) and Med-PALM (Liu et al., 2023c) are able to answer questions regarding the types of modalities, the scanned organs, and medical indicators such as opacity. They have demonstrated good performance on medical VQA datasets such as VQA-RAD (Lau et al., 2018), SLAKE (Liu et al., 2021), and Path-VQA (He et al., 2020). However, most medical questions in existing datasets are simple. MLVLMs have not been tested on a broader range of complex pathologies.

3. Methodology

Figure 1 illustrates the structure of common LVL Ms. They are based on a pretrained unimodal LLM such as Llama (Touvron et al., 2023) and Vicuna (Chiang et al., 2023). A pretrained visual encoder, such as ViT (Dosovitskiy et al., 2021) or conventional CNNs, is applied to extract image features that are projected to the text feature space by an adapter. The projected visual features are concatenated with the text prompt embeddings and fed to the LLM. The adapter usually consists of several linear layers with non-linear activations. The visual encoder and the LLM are usually frozen during training.

In our work, we choose the pretrained LLaVA-Med (Li et al., 2023a) as our model, which is a MLVLM built upon LLaVA (Liu et al., 2023b). The model structure resembles Figure 1. It uses pretrained Vicuna (Chiang et al., 2023) as the LLM and the pretrained ViT encoder from CLIP (Radford et al., 2021) as the visual encoder. The adapter is simply a trainable

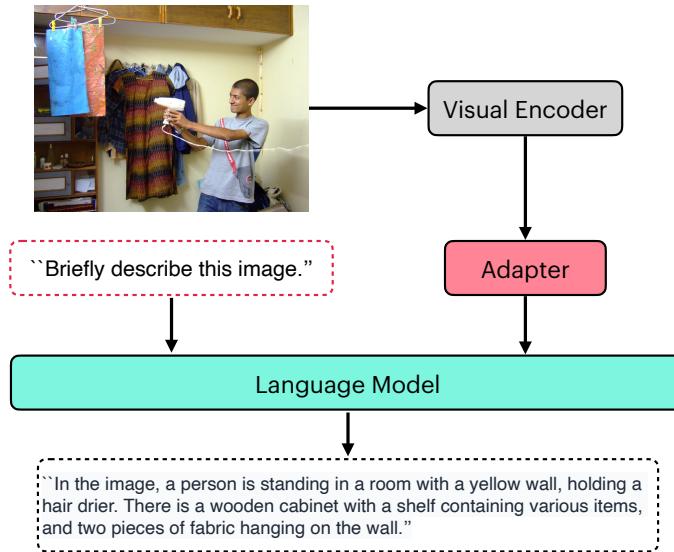


Figure 1: The structure of common LVLMs.

projection matrix. Both the visual encoder and LLM weights are frozen during training. LLaVA-Med fine-tunes LLaVA in two steps. First, it fine-tunes LLaVA to generate medical reports from input medical images. Second, it uses GPT-4 to generate various questions from the ground truth reports and fine-tunes the model to perform question answering.

Most MLVLMs are currently trained by medical VQA such that medical diagnosis can be performed by asking questions related to various pathologies; e.g., “Does this image have lung lesion?”. To reduce model hallucination and improve VQA accuracy, we propose two prompting strategies at the inference stage: (1) providing the model with detailed explanations about the queried pathologies and (2) asking the model to consider the inferences of a weak learner.

3.1 Prompting With Detailed Explanations

Given imbalanced training data, MLVLMs might not adequately be able to learn the features of the minority pathologies. To compensate for insufficient training, we provide a detailed explanation of the queried pathology as a prompt at the inference stage. The explanation briefly defines the pathology and lists several key findings in medical images that may indicate its existence. An example is shown in Figure 2. The model is informed that Pulmonary Edema is defined as the accumulation of fluid in the lungs. Then several chest X-ray findings that may suggest its existence are provided. The model can determine if the given image has Pulmonary Edema by linking the given findings with the image features.

Prompt templates for a number of pathologies are listed in Section A.

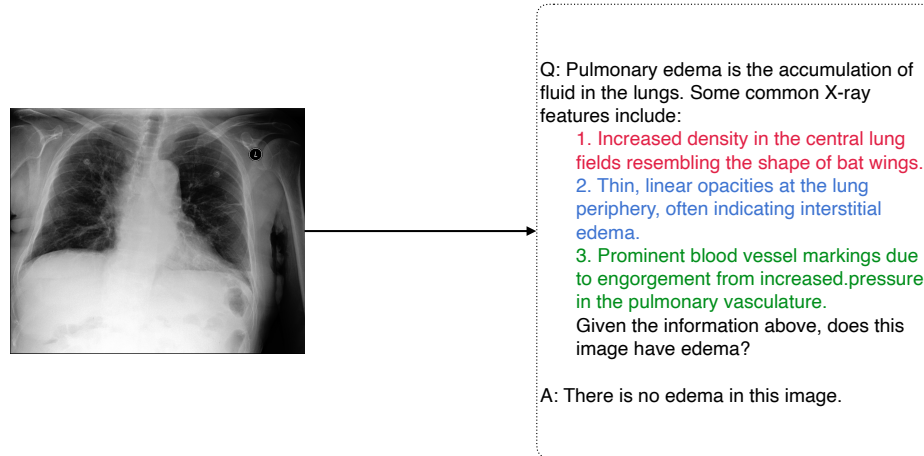


Figure 2: An example of including pathology explanations when prompting an MLVLM for medical VQA.

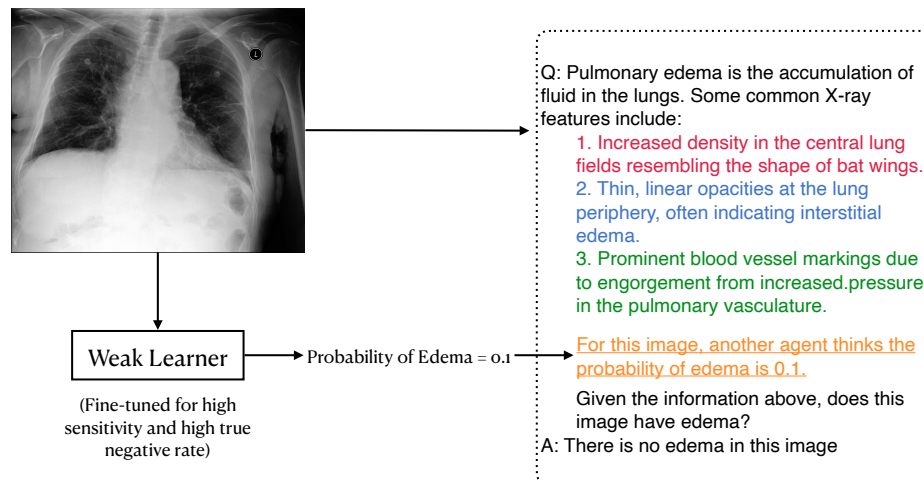


Figure 3: Example of prompting an MLVLM for medical VQA using both pathology explanations and reference predictions from a weak learner.

3.2 Prompting With Detailed Explanations and Weak Learners

Data re-sampling is a commonly-used strategy to deal with imbalanced datasets that are responsible for the tendency of traditional image classification models to return negative predictions for minority pathologies. Models trained on re-sampled datasets often exhibit improvements in Precision and Recall scores; however, this strategy may not be suitable to MLVLMs for two reasons. First, it is difficult to balance a dataset containing many categories of pathologies. Second, MLVLMs usually demand much larger datasets and fine-tuning is also expensive.

One can nevertheless enable MLVLMs to benefit by leveraging small models trained on re-sampled datasets. Our method resembles multiagent LLM systems, such as Du et al. (2023), where multiple LLMs debate each other and hallucination can be corrected by referring to the generated outputs of other models. Given that traditional image classifiers are smaller, it is feasible to train multiple small classifiers each of which is trained on re-sampled datasets of a particular pathology. Those models can be further fine-tuned to optimize a single aspect, such as fewer false positives (FP) or fewer false negatives (FN). The classifiers are applied to the medical images and return preliminary predictions. These predictions are selectively included in the prompts as references for the MLVLM. Hence, MLVLMs can benefit indirectly from the nuanced understanding that these specialized models can provide. This method is meaningful because clinicians usually must balance the trade-off between overtreatment and undertreatment when making healthcare decisions. For instance, they may prefer models having a low FP rate if the cost of overtreatment is higher than that of undertreatment.

An example is shown in Figure 3, which queries about the presence of Edema. We first provide the model with the detailed explanation of Edema. Then, we use the weak learner to suppress the FPs. The image is input to an Edema classifier that has been fine-tuned on a balanced dataset for high sensitivity and high true negative (TN) rate. If its prediction is negative, we append after the pathology explanation the prompt “For this image, another agent thinks the probability of Edema is 0.1”. Instead of using the actual predicted probability, the probability value is manually chosen because the decision threshold has been fine-tuned and is no longer 0.5. We do not use a zero probability value because we do not want the model overly to trust the weak learner. Although in this example our goal is only to reduce FPs, our strategy can also be applied to reduce FNs, simply by fine-tuning the classifier for a high true positive (TP) rate and applying the prompt in the case of positive predictions.

4. Empirical Study

4.1 Datasets

LLaVA-Med is pretrained on the PMC-15M dataset (Zhang et al., 2024), which contains image-text pairs of multiple modalities; e.g., CT, MRI, X-ray, etc. In the first stage, 467,710 image-report pairs were selected for training. In the second stage, 56,708 question-answer pairs were created from the data of the first stage to fine-tune the model. Table 1 shows the count of reports in the LLaVA-Med training data (second stage) that mention one of the

Pathology	+Cases
Atelectasis	64
Cardiomegaly	31
Consolidation	335
Edema	1,276
Pleural Effusion	260

Table 1: Positive (+) case counts for the 5 test pathologies in the LLaVA-Med training set.

Category	MIMIC-CXR-JPG (5,159)		Chexpert (668)	
	+Cases	−Cases	+Cases	−Cases
Atelectasis	1,034	4,125	178	490
Cardiomegaly	1,258	3,901	175	493
Consolidation	326	4,833	35	633
Edema	959	4,200	85	583
Enlarged Cardiomedastinum	200	4,959	298	370
Fracture	167	4,992	6	662
Lung Lesion	202	4,957	14	654
Lung Opacity	1,561	3,598	310	358
Pleural Effusion	1,542	3,617	120	548
Pleural Other	119	5,040	8	660
Pneumonia	539	4,620	14	654
Pneumothorax	144	5,015	10	658
Support Devices	1,457	3,702	315	353

Table 2: Splits of positive (+) and negative (−) cases (‘uncertain’ is regarded as negative) for the 13 finding categories in the MIMIC-CXR-JPG and Chexpert test sets.

five test pathologies as positive. Relative to the total amount of data, all five categories are minorities.

To assess the zero-shot performance of the MLVLM, we used the MIMIC-CXR-JPG (Goldberger et al., 2000) and Chexpert (Irvin et al., 2019) chest X-ray test sets. They include 5,159 and 668 images, respectively. Neither dataset overlaps with PMC-15M.

MIMIC-CXR-JPG includes images and medical reports covering 13 categories of findings: Atelectasis, Cardiomegaly, Consolidation, Edema, Enlarged Cardiomedastinum, Fracture, Lung Lesion, Lung Opacity, Pleural Effusion, Pneumonia, Pneumothorax, Pleural Other, and Support Devices. The raw reports are parsed and rough image-level tags are automatically generated by a rule-based approach (Irvin et al., 2019). Each label contains four values: 1 (positive), 0 (negative), −1 (uncertain), and missing. For simplicity, we treat both uncertain and missing as negative. We also use the MIMIC-CXR-JPG training set, which contains 227,827 chest X-rays with reports, to train the weak learner models.

Prompt	Template
PT1	“Does this image have {target}?”
PT2	“{explanation} Given the information above, does this image have {target}?”
PT3	“{explanation} For this image, another agent thinks the probability that it has {target} is {n} percent. Given the information above, does this image have {target}?”

Table 3: The Prompt Templates (PTs). {target} is the pathology cited in the questions. {explanation} contains a pathology explanation among those listed in Section A. {n} is the probability associated with the weak learner.

Chexpert covers the same 13 categories as MIMIC-CXR-JPG. However, it does not include medical reports and has only image-level labels. There is no overlap between MIMIC-CXR-JPG and Chexpert.

Table 2 shows the split of pathology categories (excluding normal) in the MIMIC-CXR-JPG and Chexpert test sets. Clearly, almost all pathology categories are minor classes with much fewer positive than negative occurrences.

For our main testing regimen, we selected the five pathologies in the Chexpert Competition (Irvin et al., 2019), Atelectasis, Cardiomegaly, Consolidation, Edema, and Pleural Effusion.

4.2 Implementation Details

As was mentioned in Section 3, we use the pretrained LLaVA-Med MLVLM without any further fine-tuning. We convert the classification task into a VQA task by using the prompt template shown in Row 1 of Table 3, which we name Prompt Template 1 (PT1). We first run the pretrained LLaVA-Med with PT1. Next, we incorporate pathology explanations (Row 2 of Table 3), yielding Prompt Template 2 (PT2). Finally, we integrate the predictions of weak learners into the prompts (Row 3 of Table 3), resulting in Prompt Template 3 (PT3).

As will be justified by our experiments, our weak learner is designed to suppress FP predictions. To this end, we use the pretrained ResNet50 (He et al., 2016). For each pathology, the training dataset was sampled such that the ratio of positive and negative cases is 2 : 1. The model was trained for 10 epochs with a $1e - 4$ learning rate. The training process was monitored using the AUC score and the one with the highest validation AUC was kept. Then, the decision threshold d was fine-tuned to optimize a weighted sum of Specificity and Negative Predictive Value (NPV); i.e.,

$$d = w_1 \frac{TN}{TN + FP} + w_2 \frac{TN}{TN + FN}, \quad (1)$$

where weights w_1 and w_2 are preset to 0.2 and 0.8, respectively. The medical images were input to the weak learners to obtain preliminary predictions for each pathology and only the negative predictions were selected to craft the PT3 prompts.

The responses returned by LLaVA-Med can take various forms, such as “This image has Edema”, “Edema is found”, “The fluid in the lung indicates Edema”, etc. An off-the-shelf

Pathology	Metric	MIMIC-CXR-JPG		Chexpert	
		PT1	PT2	PT1	PT2
Atelectasis	Precision	19.5	20.0	30.5	26.5
	Recall	41.5	92.9	44.4	91.6
	F1	26.5	33.0	36.5	41.0
Cardiomegaly	Precision	25.8	24.6	27.1	26.0
	Recall	22.5	89.4	20.0	86.3
	F1	24.0	38.6	23.0	40.0
Consolidation	Precision	6.8	6.3	6.0	5.2
	Recall	42.3	98.5	40.0	97.1
	F1	11.7	11.9	10.4	9.8
Edema	Precision	19.6	18.5	11.7	13.7
	Recall	36.0	72.7	29.4	76.5
	F1	25.4	29.5	16.8	23.2
Pleural Effusion	Precision	30.4	30.0	22.3	17.9
	Recall	42.8	92.7	49.2	90.0
	F1	35.6	45.3	30.7	29.9

Table 4: LLaVA-Med VQA performance evaluated by Precision, Recall, and F1 (%) scores of five pathologies on the MIMIC-CXR-JPG and Chexpert test datasets.

Llama-7B (Touvron et al., 2023) serves to summarize long responses into Yes/No answers such that accuracies could easily be computed.

4.3 Results

To demonstrate the efficacy of our prompting strategies, starting from the PT1 baseline, the pathology explanations were provided first (strategy PT2) and then, based on the results, weak learners were introduced to improve performance on specific aspects, resulting in strategy PT3.

PT2: Adding Pathology Explanations Table 4 reports Precision, Recall, and F1 scores of the PT1 and PT2 strategies on the MIMIC-CXR-JPG and Chexpert test sets.¹ On MIMIC-CXR-JPG, after adding pathology explanations, the F1 scores increased for detecting Atelectasis, Cardiomegaly, Edema, and Pleural Effusion, albeit only minimally for Consolidation. On Chexpert, after adding pathology explanations, the F1 scores for detecting Atelectasis, Cardiomegaly, and Edema increased, whereas they did not for Consolidation and Pleural Effusion. The Precision and Recall scores reveal that adding explanations generally leads to a large increase in Recall, but only minimally influences Precision. For minority

1. The AUC and ROC scores commonly reported in the literature to assess the performances of most medical image classification models on the MIMIC-CXR-JPG and Chexpert datasets are unsuitable in our context because MLVLMs output text rather than probabilities.

Pathology	TP	FP	FN
Atelectasis	163	453	15
Cardiomegaly	151	430	24
Consolidation	28	557	7
Edema	65	410	20
Pleural Effusion	108	495	12

Table 5: True positive (TP), false positive (FP), and false negative (FN) counts of LLaVA-Med with the PT2 strategy on the Chexpert test set.

Pathology	Metric	PT2	PT3
Atelectasis	Precision	26.5	28.8
	Recall	91.6	83.1
	F1	41.0	42.8
Cardiomegaly	Precision	26.0	38.1
	Recall	86.3	79.4
	F1	40.0	51.5
Consolidation	Precision	5.2	7.5
	Recall	97.1	34.3
	F1	9.8	12.2
Edema	Precision	13.7	36.8
	Recall	76.5	50.6
	F1	23.2	42.6
Pleural Effusion	Precision	17.9	25.0
	Recall	90.0	85.0
	F1	29.9	38.8

Table 6: Diagnostic accuracies of LLaVA-Med with the PT2 and PT3 strategies on the Chexpert test set.

pathologies such as Consolidation whose F1 score is dominated by low Precision, improving the Recall would not have much effect. Thus, PT2’s performance bottleneck is Precision.

PT3: Referring to Weak Learners Going beyond our PT2 strategy, we applied our PT3 strategy to further improve diagnostic accuracy. Table 5 provides the TP, FP, and FN prediction counts of LLaVA-Med on the Chexpert test set using the PT2 strategy. Note the large number of FP cases. Hence, we designed our weak learners to suppress FP predictions. Table 6 compares the performance on Chexpert before and after referring to the weak learner. It shows that the F1 prediction accuracy can be substantially increased by introducing weak learner predictions into the prompts. The F1 scores of Cardiomegaly, Edema, and Pleural Effusion increase by 0.115, 0.194 and 0.089, respectively. To further demonstrate the efficacy

Pathology	PT2	PT3
Atelectasis	453	365
Cardiomegaly	430	226
Consolidation	557	149
Edema	410	88
Pleural Effusion	495	304

Table 7: FP counts of LLaVA-Med with the PT2 and PT3 strategies on the Chexpert test set.

Pathology	Metric	MIMIC-CXR-JPG			Chexpert		
		PT1	PT2	PT3	PT1	PT2	PT3
Enlarged Cardiome-diastinum	Precision	4.3	3.9	5.0	49.3	44.1	49.4
	Recall	15.0	89.0	53.5	12.4	85.2	59.1
	F1	6.7	7.4	9.1	19.8	58.1	53.8
Lung Lesion	Precision	3.9	3.9	4.2	2.0	2.1	2.9
	Recall	77.2	100.0	66.3	71.4	100.0	92.9
	F1	7.4	7.5	8.0	3.9	4.1	5.7
Lung Opacity	Precision	31.4	30.4	31.9	50.0	47.2	51.4
	Recall	67.6	88.8	84.1	70.3	90.7	84.8
	F1	42.8	45.3	46.2	58.5	62.1	63.3
Pneumonia	Precision	11.4	10.5	12.3	2.4	1.7	6.3
	Recall	20.0	74.6	18.0	21.4	57.1	28.6
	F1	14.6	18.4	14.6	4.4	3.4	10.4
Pneumothorax	Precision	3.0	2.6	3.6	0.0	1.7	2.0
	Recall	16.7	78.5	50.7	0.0	90.0	50.0
	F1	5.1	5.1	6.8	0.0	3.3	3.8

Table 8: LLaVA-Med VQA performance on the MIMIC-CXR-JPG and Chexpert test sets for another 5 pathologies.

of our PT3 strategy, Table 7 compares the FP predictions of the PT2 and PT3 strategies. The reduction of FP cases is noteworthy, especially on Edema, for which the FP count is reduced by 78.5% (322).

Additional VQA Experiments Table 8 shows the results of applying the PT1, PT2, and PT3 strategies with LLaVA-Med on the MIMIC-CXR-JPG and Chexpert datasets across another five medical findings: Enlarged Cardiome-diastinum, Lung Lesion, Lung Opacity, Pneumonia, and Pneumothorax. Providing pathology explanations (PT2) generally yields better results over the PT1 baseline, albeit inconsistently. Introducing weak learner

Pathology	Radiologist	(Tiu et al., 2022)	PT1	PT3
Atelectasis	69.2	64.6	26.5	41.3
Cardiomegaly	67.8	74.3	24.0	51.5
Consolidation	38.5	33.3	11.7	12.2
Edema	58.3	60.2	25.4	42.6
Pleural Effusion	73.7	70.4	35.5	46.8

Table 9: F1 scores (%) on 5 pathologies in the Chexpert test set, including for the radiologist diagnoses, the state-of-the-art benchmark (Tiu et al., 2022), as well as LLaVA-Med VQA with the PT1 scenario and the PT3 scenario, which is the best result achieved by applying both our prompting strategies.

Model	POPE Adversarial			POPE Popular			POPE Random		
	Precision	Recall	F1	Precision	Recall	F1	Precision	Recall	F1
LLaVA	91.0	78.8	84.5	95.2	78.8	86.2	97.4	78.8	87.1
with referral	88.4	85.7	87.0	92.8	85.7	89.0	97.3	85.7	91.1
MiniGPT-v2	88.2	77.2	82.3	92.7	77.2	84.2	97.2	77.2	86.1
with referral	86.8	84.2	85.5	91.9	84.2	87.9	97.3	84.2	90.3

Table 10: Comparison of POPE scores for LVLm models with and without referring to the predictions of weak learners.

references (PT3) yields only limited increases in Precision, but large decreases in Recall. Generally, it offers insignificant improvement. Enlarged Cardiome-diastinum, Lung Lesion, Pneumonia, and Pneumothorax are minor categories and all our experimental settings, including for the weak learner, fail to learn them. Prompting is apparently unhelpful in such situations.

SOTA Benchmark Tiu et al. (2022) report F1 scores for detecting Atelectasis, Cardiomegaly, Consolidation, Edema, and Pleural Effusion on the Chexpert dataset using their deep learning model, as well as for the performance of radiologists. Their work offers a state-of-the-art chest X-ray diagnosis benchmark. Table 9 compares the F1 scores of radiologists, the model of Tiu et al. (2022), and LLaVA-Med. It shows that LLaVA-Med’s VQA performance of with the baseline PT1 strategy is unsatisfactory, rendering the model far from being deployable in clinical practice. However, while still underperforming radiologists, our PT3 strategy yields a significant improvement, especially on Atelectasis, Cardiomegaly, and Edema for which the F1 score increases by approximately 17% to 21%.

Application to General Domain LVLmS Our prompt strategies can also be applied to general domain LVLmS. We studied the performance of LLaVA (Liu et al., 2023b) and MiniGPT-v2 (Zhu et al., 2023) using POPE metrics (Li et al., 2023c), which evaluate the hallucination of LVLmS by asking questions about the presence of objects. The POPE scores

of LLaVA and MiniGPT-v2 have high Precision and low Recall. Hence, our weak learner strategy can be used to reduce the FN predictions. We selected an off-the-shelf Fast-RCNN (Girshick, 2015) as the weak learner, fine-tuned the detection threshold of bounding box scores to achieve high Recall, and introduced the positive predictions of the weak learner into the prompts. The results in Table 10 show that the Recall scores across three POPE categories increased by around 7% (Precision scores decrease slightly), thus improving the F1 scores.

5. Conclusions and Discussion

We have tested the visual question answering abilities of the LLaVA-Med medical large vision-language model when applied to the diagnosis of pathologies. Our results show that the model has unsatisfactory performance when asked questions regarding the presence of complex pathologies. We proposed two prompt engineering strategies to improve the visual question answering accuracy of the model: providing explanations of pathologies and referring to the predictions of weak learners. The first strategy helps the model understand minority pathologies that it does not learn well in the training stage. The second strategy can help improve diagnostic accuracy in specific ways; e.g., by suppressing false positives. This strategy can also be applied to LVLMs in other, non-medical domains.

However, our two strategies are not effective on pathologies with extremely scarce data. For example, providing text explanations for Consolidation, Fracture, Lung Lesion, Pneumonia, and Pneumothorax may not suffice since the visual encoder does not adequately learn meaningful visual features. Moreover, the data may not suffice to adequately train weak learners. A promising direction for future research would be to devise a strategy for handle these rare categories. Retrieval Augmented Generation (RAG) could be a potential solution. In addition to textual explanation of a pathology, for instance, typical example images can be provided to help the model make diagnostic decisions.

Appendix A. Pathology Explanations

The explanations of the five pathologies are as follows:

Atelectasis: Atelectasis refers to the partial or complete collapse of a lung or a section of lung. The features of atelectasis on an X-ray can vary depending on the cause and extent of the collapse. Some common X-ray features include: 1. The affected area may appear denser or whiter than normal lung tissue due to the collapse, leading to increased opacity on the X-ray. 2. The affected portion of the lung may appear smaller or compressed compared to the surrounding healthy lung tissue. 3. Atelectasis can cause a shift or displacement of nearby structures, such as the trachea or heart, toward the affected area. 4. In obstructive atelectasis (caused by a blockage in the airways), there might be signs of hyperinflation in the unaffected areas of the lung and a visible blockage or narrowing in the affected bronchus. 5. Linear or band-like opacities may be visible, often referred to as plate or band atelectasis, which can occur due to the collapse of small airways. Given the information above, does this image have Atelectasis?

Cardiomegaly: Cardiomegaly is enlargement of the heart. The definition is when the transverse diameter of the cardiac silhouette is greater than or equal to 50% of the transverse diameter of the chest (increased cardiothoracic ratio) on a posterior-anterior projection of a chest radiograph or a computed tomography. Given the information above, does this image have Cardiomegaly?

Consolidation: Consolidation on an X-ray refers to the filling of the lung’s air spaces with fluid inflammatory exudate, or cellular material. Typical X-ray findings suggesting consolidation include: 1. Areas of increased density in the lung tissue, appearing as an opaque or hazy patch on the X-ray. Given the information above, does this image have Consolidation?

Edema: Pulmonary edema is the accumulation of fluid in the lungs. Some common X-ray features include: 1. Increased density in the central lung fields resembling the shape of bat wings. 2. Thin, linear opacities at the lung periphery, often indicating interstitial edema. 3. Prominent blood vessel markings due to engorgement from increased pressure in the pulmonary vasculature. Given the information above, does this image have Edema?

Pleural Effusion: Pleural effusion is the accumulation of fluid in between the parietal and visceral pleura. Some common X-ray features include: 1. blunting of the costophrenic/cardiophrenic angle. 2. fluid within the horizontal or oblique fissures. 3. meniscus is seen. 4. mediastinal shift occurs away from the effusion.

References

- Davide Caffagni, Federico Cocchi, Nicholas Moratelli, Sara Sarto, Marcella Cornia, Lorenzo Baraldi, and Rita Cucchiara. Wiki-LLaVA: Hierarchical retrieval-augmented generation for multimodal LLMs. *arXiv Preprint arXiv:2404.15406*, 2024.
- Wei-Lin Chiang, Zhuohan Li, Zi Lin, Ying Sheng, Zhanghao Wu, Hao Zhang, Lianmin Zheng, Siyuan Zhuang, Yonghao Zhuang, Joseph E. Gonzalez, Ion Stoica, and Eric P. Xing. Vicuna: An open-source chatbot impressing GPT-4 with 90%* ChatGPT quality, March 2023. URL <https://lmsys.org/blog/2023-03-30-vicuna/>.
- Alexey Dosovitskiy, Lucas Beyer, Alexander Kolesnikov, Dirk Weissenborn, Xiaohua Zhai, Thomas Unterthiner, Mostafa Dehghani, Matthias Minderer, Georg Heigold, Sylvain Gelly, Jakob Uszkoreit, and Neil Houlsby. An image is worth 16x16 words: Transformers for image recognition at scale. In *9th International Conference on Learning Representations, ICLR 2021, Virtual Event, Austria, May 3-7, 2021*. OpenReview.net, 2021.
- Yilun Du, Shuang Li, Antonio Torralba, Joshua B Tenenbaum, and Igor Mordatch. Improving factuality and reasoning in language models through multiagent debate. *arXiv Preprint arXiv:2305.14325*, 2023.
- Alessandro Favero, Luca Zancato, Matthew Trager, Siddharth Choudhary, Pramuditha Perera, Alessandro Achille, Ashwin Swaminathan, and Stefano Soatto. Multi-modal hallucination control by visual information grounding. *arXiv Preprint arXiv:2403.14003*, 2024.

- Ross Girshick. Fast R-CNN. In *Proceedings of the IEEE International Conference on Computer Vision*, pages 1440–1448, 2015.
- Ary L Goldberger, Luis AN Amaral, Leon Glass, Jeffrey M Hausdorff, Plamen Ch Ivanov, Roger G Mark, Joseph E Mietus, George B Moody, Chung-Kang Peng, and H Eugene Stanley. PhysioBank, PhysioToolkit, and PhysioNet: Components of a new research resource for complex physiologic signals. *circulation*, 101(23):e215–e220, 2000.
- Kaiming He, Xiangyu Zhang, Shaoqing Ren, and Jian Sun. Deep residual learning for image recognition. In *Proceedings of the IEEE Conference on Computer Vision and Pattern Recognition*, pages 770–778, 2016.
- Xuehai He, Yichen Zhang, Luntian Mou, Eric Xing, and Pengtao Xie. PathVQA: 30000+ questions for medical visual question answering. *arXiv Preprint arXiv:2003.10286*, 2020.
- Hongyu Hu, Jiyuan Zhang, Minyi Zhao, and Zhenbang Sun. CIEM: Contrastive instruction evaluation method for better instruction tuning. *arXiv Preprint arXiv:2309.02301*, 2023.
- Jeremy A. Irvin, Pranav Rajpurkar, Michael Ko, Yifan Yu, Silviana Ciurea-Ilcus, Chris Chute, Henrik Marklund, Behzad Haghgoo, Robyn L. Ball, Katie S. Shpanskaya, Jayne Seekins, David Andrew Mong, Safwan S. Halabi, Jesse K. Sandberg, Ricky Jones, David B. Larson, C. Langlotz, Bhavik N. Patel, Matthew P. Lungren, and A. Ng. CheXpert: A large chest radiograph dataset with uncertainty labels and expert comparison. In *AAAI Conference on Artificial Intelligence*, 2019.
- Jitesh Jain, Jianwei Yang, and Humphrey Shi. Vcoder: Versatile vision encoders for multimodal large language models. *arXiv Preprint arXiv:2312.14233*, 2023.
- Jason J Lau, Soumya Gayen, Asma Ben Abacha, and Dina Demner-Fushman. A dataset of clinically generated visual questions and answers about radiology images. *Scientific data*, 5(1):1–10, 2018.
- Sicong Leng, Hang Zhang, Guanzheng Chen, Xin Li, Shijian Lu, Chunyan Miao, and Lidong Bing. Mitigating object hallucinations in large vision-language models through visual contrastive decoding. *arXiv Preprint arXiv:2311.16922*, 2023.
- Chunyuan Li, Cliff Wong, Sheng Zhang, Naoto Usuyama, Haotian Liu, Jianwei Yang, Tristan Naumann, Hoifung Poon, and Jianfeng Gao. LLaVA-Med: Training a large language-and-vision assistant for biomedicine in one day. *arXiv Preprint arXiv:2306.00890*, 2023a.
- Junnan Li, Dongxu Li, Silvio Savarese, and Steven Hoi. BLIP-2: Bootstrapping language-image pre-training with frozen image encoders and large language models. In *International Conference on Machine Learning*, 2023b.
- Yifan Li, Yifan Du, Kun Zhou, Jinpeng Wang, Xin Zhao, and Ji-Rong Wen. Evaluating object hallucination in large vision-language models. In Houda Bouamor, Juan Pino, and Kalika Bali, editors, *Proceedings of the 2023 Conference on Empirical Methods in Natural Language Processing*, pages 292–305, Singapore, December 2023c. Association for Computational Linguistics. .

- Bo Liu, Li-Ming Zhan, Li Xu, Lin Ma, Yan Yang, and Xiao-Ming Wu. Slake: A semantically-labeled knowledge-enhanced dataset for medical visual question answering. In *2021 IEEE 18th International Symposium on Biomedical Imaging (ISBI)*, 2021.
- Fuxiao Liu, Kevin Lin, Linjie Li, Jianfeng Wang, Yaser Yacoob, and Lijuan Wang. Mitigating hallucination in large multi-modal models via robust instruction tuning. In *The Twelfth International Conference on Learning Representations*, 2023a.
- Hanchao Liu, Wenyuan Xue, Yifei Chen, Dapeng Chen, Xiutian Zhao, Ke Wang, Liping Hou, Rongjun Li, and Wei Peng. A survey on hallucination in large vision-language models. *arXiv Preprint arXiv:2402.00253*, 2024.
- Haotian Liu, Chunyuan Li, Qingyang Wu, and Yong Jae Lee. Visual instruction tuning. In *Neural Information Processing Systems*, 2023b.
- Yinhan Liu, M. Wang, X. Liu, W. Chang, M. Sun, and P. Li. Large language models encode clinical knowledge. *Nature*, 603:589–593, 2023c. .
- Holy Lovenia, Wenliang Dai, Samuel Cahyawijaya, Ziwei Ji, and Pascale Fung. Negative object presence evaluation (NOPE) to measure object hallucination in vision-language models. *arXiv Preprint arXiv:2310.05338*, 2023.
- OpenAI. ChatGPT blog, 2022. <https://openai.com/blog/chatgpt>.
- OpenAI et al. GPT-4 technical report. *arXiv Preprint arXiv:2303.08774*, 2023.
- Yusu Qian, Haotian Zhang, Yinfei Yang, and Zhe Gan. How easy is it to fool your multimodal LLMs? An empirical analysis on deceptive prompts. *arXiv Preprint arXiv:2402.13220*, 2024.
- Alec Radford, Jong Wook Kim, Chris Hallacy, Aditya Ramesh, Gabriel Goh, Sandhini Agarwal, Girish Sastry, Amanda Askell, Pamela Mishkin, Jack Clark, Gretchen Krueger, and Ilya Sutskever. Learning transferable visual models from natural language supervision. In Marina Meila and Tong Zhang, editors, *Proceedings of the 38th International Conference on Machine Learning*, volume 139 of *Proceedings of Machine Learning Research*, pages 8748–8763. PMLR, 18–24 Jul 2021.
- Anna Rohrbach, Lisa Anne Hendricks, Kaylee Burns, Trevor Darrell, and Kate Saenko. Object hallucination in image captioning. In Ellen Riloff, David Chiang, Julia Hockenmaier, and Jun’ichi Tsujii, editors, *Proceedings of the 2018 Conference on Empirical Methods in Natural Language Processing*, pages 4035–4045, Brussels, Belgium, October–November 2018. Association for Computational Linguistics. .
- Karan Singhal, Tao Tu, Juraj Gottweis, Rory Sayres, Ellery Wulczyn, Le Hou, Kevin Clark, Stephen Pfohl, Heather Cole-Lewis, Darlene Neal, Mike Schaekermann, Amy Wang, Mohamed Amin, Sami Lachgar, Philip Mansfield, Sushant Prakash, Bradley Green, Ewa Dominowska, Blaise Aguera y Arcas, Nenad Tomasev, Yun Liu, Renee Wong, Christopher Semturs, S. Sara Mahdavi, Joelle Barral, Dale Webster, Greg S. Corrado, Yossi Matias, Shekoofeh Azizi, Alan Karthikesalingam, and Vivek Natarajan. Towards expert-level

- medical question answering with large language models. *arXiv Preprint arXiv:2305.09617*, 2023.
- Zhiqing Sun, Sheng Shen, Shengcao Cao, Haotian Liu, Chunyuan Li, Yikang Shen, Chuang Gan, Liang-Yan Gui, Yu-Xiong Wang, Yiming Yang, Kurt Keutzer, and Trevor Darrell. Aligning large multimodal models with factually augmented RLHF. *arXiv Preprint arXiv:2309.14525*, 2023a.
- Zhiqing Sun, Sheng Shen, Shengcao Cao, Haotian Liu, Chunyuan Li, Yikang Shen, Chuang Gan, Liang-Yan Gui, Yu-Xiong Wang, Yiming Yang, et al. Aligning large multimodal models with factually augmented RLHF. *arXiv Preprint arXiv:2309.14525*, 2023b.
- Ekin Tiu, Ellie Talius, Pujan Patel, Curtis P Langlotz, Andrew Y Ng, and Pranav Rajpurkar. Expert-level detection of pathologies from unannotated chest X-ray images via self-supervised learning. *Nature Biomedical Engineering*, 6(12):1399–1406, 2022.
- Hugo Touvron, Thibaut Lavril, Gautier Izacard, Xavier Martinet, Marie-Anne Lachaux, Timothée Lacroix, Baptiste Rozière, Naman Goyal, Eric Hambro, Faisal Azhar, Aurelien Rodriguez, Armand Joulin, Edouard Grave, and Guillaume Lample. LLaMA: Open and efficient foundation language models. *arXiv Preprint arXiv:2302.13971*, 2023.
- Boshi Wang, Sewon Min, Xiang Deng, Jiaming Shen, You Wu, Luke Zettlemoyer, and Huan Sun. Towards understanding chain-of-thought prompting: An empirical study of what matters. In Anna Rogers, Jordan Boyd-Graber, and Naoaki Okazaki, editors, *Proceedings of the 61st Annual Meeting of the Association for Computational Linguistics (Volume 1: Long Papers)*, pages 2717–2739, Toronto, Canada, July 2023. Association for Computational Linguistics. .
- Renrui Zhang, Jiaming Han, Chris Liu, Peng Gao, Aojun Zhou, Xiangfei Hu, Shilin Yan, Pan Lu, Hongsheng Li, and Yu Qiao. LLaMA-Adapter: Efficient fine-tuning of language models with zero-init attention. *arXiv Preprint arXiv:2303.16199*, 2023.
- Sheng Zhang, Yanbo Xu, Naoto Usuyama, Hanwen Xu, Jaspreet Bagga, Robert Tinn, Sam Preston, Rajesh Rao, Mu Wei, Naveen Valluri, Cliff Wong, Andrea Tupini, Yu Wang, Matt Mazzola, Swadheen Shukla, Lars Liden, Jianfeng Gao, Matthew P. Lungren, Tristan Naumann, Sheng Wang, and Hoifung Poon. BiomedCLIP: A multimodal biomedical foundation model pretrained from fifteen million scientific image-text pairs. *arXiv Preprint arXiv:2303.00915*, 2024.
- Linxi Zhao, Yihe Deng, Weitong Zhang, and Quanquan Gu. Mitigating object hallucination in large vision-language models via classifier-free guidance. *arXiv Preprint arXiv:2402.08680*, 2024.
- Ge Zheng, Bin Yang, Jiajin Tang, Hong-Yu Zhou, and Sibe Yang. DDCoT: Duty-distinct chain-of-thought prompting for multimodal reasoning in language models. In A. Oh, T. Neumann, A. Globerson, K. Saenko, M. Hardt, and S. Levine, editors, *Advances in Neural Information Processing Systems*, volume 36, pages 5168–5191. Curran Associates, Inc., 2023.

Yiyang Zhou, Chenhang Cui, Jaehong Yoon, Linjun Zhang, Zhun Deng, Chelsea Finn, Mohit Bansal, and Huaxiu Yao. Analyzing and mitigating object hallucination in large vision-language models. In *The Twelfth International Conference on Learning Representations*, 2024.

Deyao Zhu, Jun Chen, Xiaoqian Shen, Xiang Li, and Mohamed Elhoseiny. MiniGPT-4: Enhancing vision-language understanding with advanced large language models. *arXiv Preprint arXiv:2304.10592*, 2023.